Copyright © 2014 American Scientific Publishers
All rights reserved
Printed in the United States of America

Journal of Medical Imaging and Health Informatics
Vol. 4, 58–65, 2014

Contrast Transfer Efficiency of Ultrasound Elastography—A Simulation Study

M. Kavitha[1,*], M. Ramasubba Reddy[1], and S. Suresh[2]

[1]*Biomedical Engineering Division, Department of Applied Mechanics, Indian Institute of Technology Madras, Chennai 600036, India*
[2]*Mediscan Systems, Chennai 600004, India*

Ultrasound Elastography Imaging (UEI) is one of the *in vivo* stiffness measurement methods for human tissues. Since stiffness is highly correlated with pathology of tissue, measurement of stiffness could be helpful in diagnosis of cancer in breast, thyroid, prostate and liver. UEI involves, applying a small external compression on tissue of interest and then measuring the deformation using ultrasound imaging. Contrast transfer efficiency (CTE) is defined as the ability of any imaging technique to represent the actual modulus ratio in to a reasonable image contrast. In this work, a study was carried out to investigate the contrast transfer efficiency of ultrasound Elastography Imaging (UEI) in characterizing different classes of inclusions using simulated tissue mimicking phantoms. Using finite element method, phantom was simulated with embedded inclusions of varying stiffness to represent different stages of cancer. Results show that mean CTE is comparatively better for low modulus contrast lesions than high modulus contrast lesions. Results are validated with clinical images and have good agreement with literature also.

Copyright: American Scientific Publishers

Keywords: Ultrasound Elastography, Contrast Transfer Efficiency, Finite Element Model.

1. INTRODUCTION

Ultrasound Imaging is a popular imaging modality for diagnosis of breast, prostate, liver and thyroid cancer due to its safety and low cost.[1] Though *B*-mode Ultrasound imaging is used as a screening tool in cancer diagnosis, many times it fails to detect cancerous tissue from soft tissue due to their similar echogenicity. The abnormalities such as benign and malignant cancer lesions on the other hand show much variation in their stiffness properties.[2] Hence, cancerous tissues could be diagnosed by measurements of its stiffness *in vivo*. Ultrasound Elastography is a method of imaging stiffness properties of tissues specifically related to Young's Modulus.[3,4] It is known as remote palpation and is described by Ophir 1991.[3] The principle of UEI involves acquiring and comparing ultrasound signals from tissues before and after a small external compression. When the body tissues are compressed, the softer parts deform more easily than the harder parts. The displacement or strain produced inside the tissue due to the compression is computed from the acquired ultrasound signal based on correlation techniques and displayed as an elastogram.

Ultrasound stiffness imaging methods are grouped according to the source of compression and how the local displacements are measured. Compression of tissues may be either via probe (static or quasi static),[3] by natural movements of the body like heart beat, pulsing of blood vessels,[5,6] dynamic external vibration to create shear waves within the tissue of interest called as sonoelasticity[7] or precisely by acoustic radiation force generated by ultrasound pulse.[8] They are further classified based on the method of deformation measurement either by ultrasound,[6] Magnetic Resonance Imaging[9,10] or optical methods.[11] The focus of this paper is to analyze the performance of Ultrasound Elastography Imaging (UEI) which is based on external compression.

Basically there are two types of cancer tissue namely benign and malignant depending on whether or not they can spread by invasion and metastasis. Benign lesions are those that cannot spread out by invasion. They grow only locally and they can be cured by suitable therapy where as malignant tumor invades neighboring cells, enter into blood vessels, lymphatic system and metastasize to different sites. Based on the stiffness properties, benign tumors are generally around 2 to 3 times stiffer than normal tissues and deform more for an applied compression. But malignant tumors are harder than surrounding tissues and show less deformation. Thus they show good elastic contrast than acoustic contrast and this property is used in Elastogrpahy Imaging. As these two types of lesions are stiffer than the background, they are termed as hard inclusions. Soft lesions show less stiffness than the surrounding background normal tissue. Examples

*Author to whom correspondence should be addressed.

 2156-7018/2014/4/058/008 doi:10.1166/jmihi.2014.1216

are lymph node cancer, sebaceous cyst and abscess. An abscess is a tender mass generally surrounded by a colored area from pink to deep red and the middle of an abscess is full of pus and debris.[12]

The ability of UEI, to differentiate cancer tissues from normal tissue with better contrast can be studied by measuring its contrast transfer efficiency.[13,14] Contrast transfer efficiency (CTE) is defined as the ratio of observed strain contrast to underlying modulus contrast. A theoretical model of CTE in elastography has been derived by Kallel et al.[14] for the case of uniform cylindrical inclusions embedded in infinite background. Different CTE curves have been reported for uniform cylindrical and spherical inclusions.[13–15] However, in their work, CTE is deduced for simulation software models and analytic problems. On the other hand, Bharath et al.[16] presented contrast transfer improvement for electrode displacement elastography in which they claimed the improvement of CTE for elastograms generated by local compression using electrode. The objective of this work is to study CTE of UEI in detecting inclusions of varying stiffness and corroborate with clinical patient images. Changes in CTE with respect to the true modulus contrast, depth and size of inclusion in a simulated phantom is studied. Finite element analysis using 2D mechanical deformation are presented. The results are corroborated with patient images which were captured from commercial ultrasound elastography machine.

2. THEORY

2.1. Modeling of Soft Tissue

Human soft tissue exhibits an-isotropic, non-linear and visco elastic behavior[17] where the stress and strain are time dependent. Therefore an exact modeling of the mechanical behavior of the tissue under loading is difficult and cumbersome. Such materials when subjected to loading exhibit elastic deformation only under certain assumptions. To understand the behavior of the materials, the following parameters are defined. Strain (ϵ) represents the amount of deformation induced by applied force and is defined as

$$\epsilon = \frac{\delta L}{L} \tag{1}$$

where L is the length of an object and δL is the amount of change in the object length.

Stress (σ) is force causing the deformation divided by the area to which the force is applied. For small deformations, most materials show a linear relationship between stress and strain, which is described by generalized Hooke's law as

$$\sigma_{ij} = C_{ijkl}\epsilon_{kl} \tag{2}$$

where σ_{ij} is the elastic body stress and ϵ_{kl} is strain. This law establishes the linear relationship between the components of the stress and the components of the strain at any point in the body through the material property tensor, C_{ijkl}. The subscripts i, j, k and l vary from 1 to 3 for a 3-d object. C_{ijkl} is a 4th order tensor and is known as the elastic constants of the material. A full description of the material without any further simplifying assumptions require altogether 81 elastic constants. σ_{ii} and ϵ_{kk} are uni-axial stress and strain respectively, and σ_{ij} and ϵ_{kl} are shear stress and strain respectively. Since stress and strain tensors are symmetric i.e., $\sigma_{ij} = \sigma_{ji}$, the number of independent parameters are now reduced to 36. If we further assume that the material is orthotropic, i.e., there exists 3 orthogonal planes of symmetry in the body, and isotropic i.e., the elastic constants are same at a given location for all possible choices of rectangular Cartesian co ordinates, the number of elastic components are reduced to just two which are termed as Lame parameters λ and μ. In real time, Young's modulus and Poisson's ratio are used to represent the material properties which are related to λ and μ. It can easily be shown that for uni axial compressive loading which produces a compressive stress σ and strain ϵ, the Young's modulus is

$$E = \frac{\sigma}{\epsilon} = \frac{\mu(3\lambda + 2\mu)}{\lambda + \mu} \tag{3}$$

Another important parameter derivable from Hooke's law is the Poisson's ratio ν which is defined as a measure of the transverse strain resulting from an axial strain due to compression. It is given as

$$\nu = \frac{\lambda}{2(\lambda + \mu)} \tag{4}$$

Assuming that soft tissues mainly consist of water, which is in-compressible with a Poisson's ratio of 0.5, the ν for soft tissue is assumed to be in the vicinity of 0.495.

Thus, we approximate the human soft tissue to be purely elastic, showing linear isotropic behavior and therefore, characterized by its Young's modulus.[3,17] Now, it is reduced into a continuum mechanics problem whose solution involves describing it by a set of relations valid over finite continuous geometric domains and time intervals. Because of the geometrical non-linearities and the complexity of the soft tissue model it is difficult to bring forth analytical solutions defining the system behavior as a continuous function of time. Thus for the numerical solution, the continuous problem has to be discretized, which is usually implemented using the finite element method (FEM). The solution of the continuous deformation problem is approximated to the solution obtained at the nodes of the mesh which approximates the continuous domain. The FEM is preferred over other numerical techniques because of its flexibility in allowing the analysis of structures with complex geometries with embedded in-homogeneity and boundary conditions. Hence, in this work, we used FEM for modeling the tissue as a linear elastic isotropic solid problem. The approximated model is solved by finite element method which is explained in Section 3.

Delivered by Publishing Technology to: Nanyang Technological University
IP: 101.160.35.137 On: Mon, 09 Nov 2015 20:46:17
Copyright: American Scientific Publishers

2.2. Contrast Transfer Efficiency

Ultrasound Elastography is the imaging modality in which the change in longitudinal strain was considered as indicative of change of tissue modulus assuming that the stress is uniform in the region of interest. The elastic modulus contrast is depicted as image strain contrast. Ponnekanti et al. 1995[13] defined Contrast transfer efficiency (CTE) as the ability of any imaging technique to represent the actual modulus ratio in to a reasonable image contrast. It is the performance measure of imaging technique, which quantifies how well the underlying modulus contrast is represented for various categories. Mathematically, it is given by the following expression,

$$CTE = \frac{C_s}{C_m} \tag{5}$$

$$\text{In dB, } CTE\ (\text{dB}) = |C_s\ (\text{dB})| - |C_m\ (\text{dB})| \tag{6}$$

where C_s is the observed strain contrast from images and C_m is the true modulus contrast (Modulus of inclusion/Modulus of background).

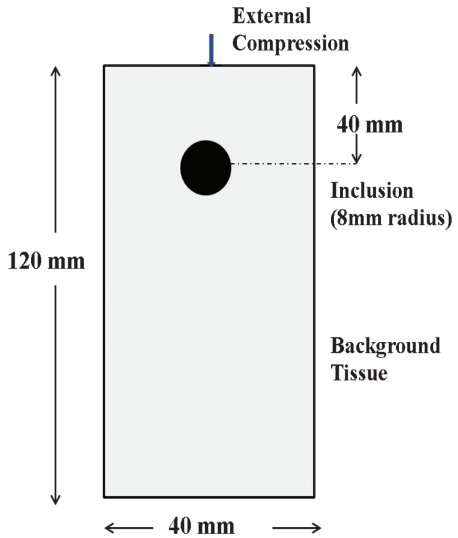


Fig. 1. Geometry of the model.

3. MATERIALS AND METHODS

3.1. Modeling

Observed strain contrast between inclusion to background in elastogram changes with location of inclusion, modulus contrast of the inclusion to background, size of the inclusion and boundary conditions.[3] It is essential to analyze the influence of above said factors on strain images for a better clinical diagnosis. In order to do this, simulated computer phantoms were modeled using finite element analysis software ANSYS (*ANSYS Inc., Canonsberg, PA, USA*). The geometry of the simulated phantom was developed by adopting the same procedure as given in Ref. [16]. The geometry is 2-D rectangular phantom (120 mm × 40 mm) with a single cylindrical inclusion of radius 8 mm and 2 mm, centered at different depths (40 mm, 60 mm, and 90 mm) were modeled. Each depth was studied as a separate case. In this model, human soft tissue was assumed as linear, elastic isotropic material. Plane strain problem was considered and meshed with quadrilateral elements of 8 nodes. Figure 1 is the schematic representation of the model.

The elastic modulus of the background was fixed at 10 kPa and that of the inclusion was varied from 0.1 kPa to 1000 kPa in finite steps for a contrast ratio of −40 dB to 40 dB. Tissue motion was induced by both displacement control and load control. For displacement control, the phantom movement was simulated for 1% of axial displacement in compression where as load control was simulated as 100 Pa pressure on the top surface of the phantom. The Poisson's ratio for both of the inclusion and background was fixed at 0.495 to model the in-compressible nature of soft tissue. Boundary conditions were given such that it matches the real time Elastography imaging and hence the lower surface of the phantom was restricted from downward movement and the sides of the rectangles were unconstrained. The problem was solved using linear solver available in ANSYS. Thereafter, simulated strain images in *y* direction (refers the axial direction of the ultrasound probe) were captured and can be referred as ideal strain images and used for calculation of CTE. Figure 2 shows sample strain images of small size inclusion for three different contrast between the inclusion and background. Grey bar represents different levels of strain. Images are cropped to highlight the inclusion portion.

3.2. Calculation of CTE

CTE is the ratio of observed contrast to true modulus contrast where as observed contrast is the ratio of the mean strain of the background to the mean strain of the inclusion. For calculating the values of observed contrast from FEA strain images, rectangular regions of interest (ROI) are selected within the inclusion and also in the background. Since CTE is highly dependent on selection ROI, it should be properly chosen. For large size inclusion (diameter is above 5 mm), the inclusion portion was selected manually and centroid was fixed. From that centroid, ROI of 60 × 60 pixels was selected, mean intensity was calculated. From the background, two such ROI of size 40 × 90 were selected and average intensity was calculated. The background ROI was selected at the same axial level of the inclusion ROI, to have uniform stress distribution (Fig. 3). For small size (diameter is below 5 mm) inclusion, inclusion ROI was chosen such that it was small enough to get mean strain of the inclusion and background ROIs were selected as same as the large size inclusion image. The trends of observed contrast and mean contrast transfer efficiency to true modulus contrast are evaluated for different modulus contrast between the inclusion and background (−40 dB to +40 dB) for different sizes of inclusions.

3.3. Clinical Elastography

The FEA results were also validated using clinical patient images. For this purpose, Ultrasound elastogram of 30 patients (16 malignant and 14 benign tumors) were collected. The type of lesion of all 30 patients were verified by biopsy. Utrasound *B* mode (prior to application of force) and elastograms (after

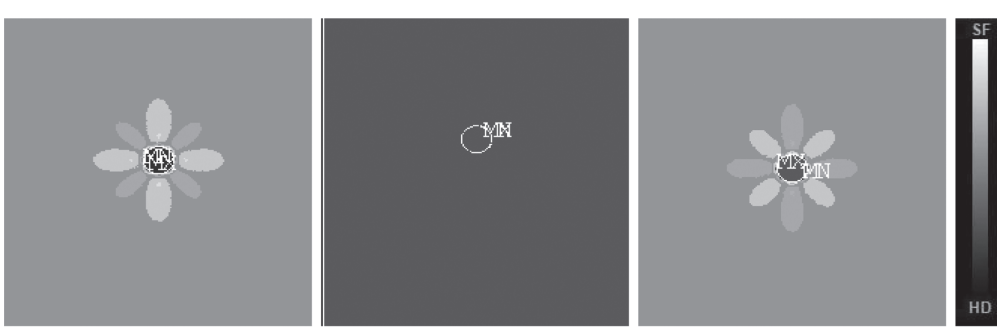


Fig. 2. Ideal strain images for true modulus ratio of (a) hard inclusion (12 dB), (b) no inclusion (0 dB) and (c) soft inclusion (−12 dB) respectively.

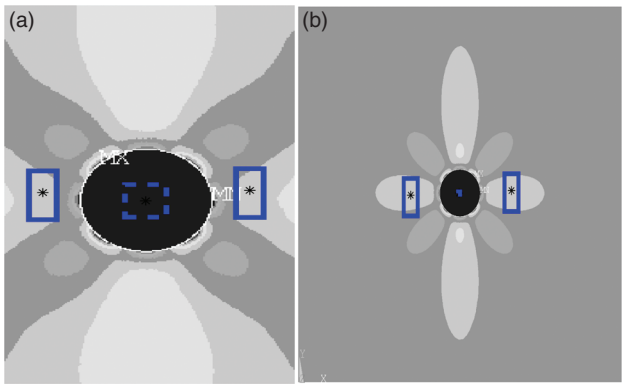


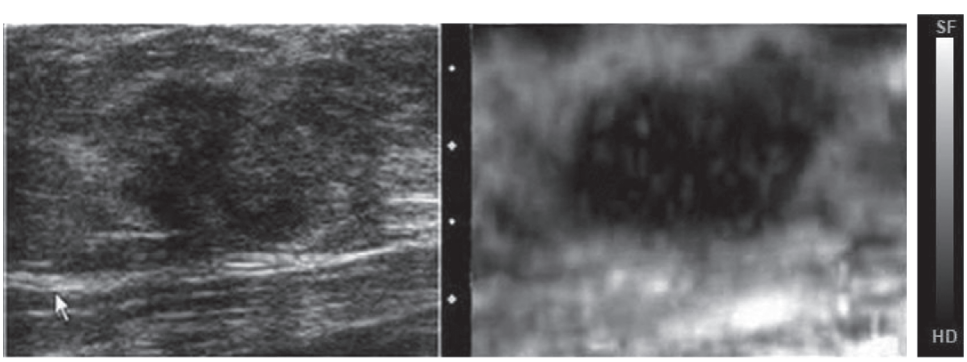
Fig. 3. ROIs in background and tumor at same level of stress (a) 8 mm radius inclusion (b) 2 mm radius inclusion.

compressive force) were acquired using *Siemens Acuson S2000* (*Siemens, Erlangen, Germany*) machine at Mediscan Systems, Chennai. Linear array transducer *9L4* with a probe frequency of 8 MHz was used. Initially, *B* mode image of the region of interest (ROI) was obtained. Once the ROI was highlighted in *B*-mode image, a slight compression was applied by pressing the transducer on the tissue of interest. Elastogram was generated by the scanner by comparing the pre-compressed and post-compressed RF signals and displayed adjacent to the *B* mode image. Figure 4 shows sample elastogram images of patients which represent the categories of benign and malignant tumors. In clinical setting, the compression applied by radiographer could not be exactly quantified. This might be applicable in Ultrasound Elastography Imaging, since the relative elastic contrast is the property of interest than quantifying the absolute elastic modulus. The relative elastic property is estimated by capturing the pre and post compression echoes.

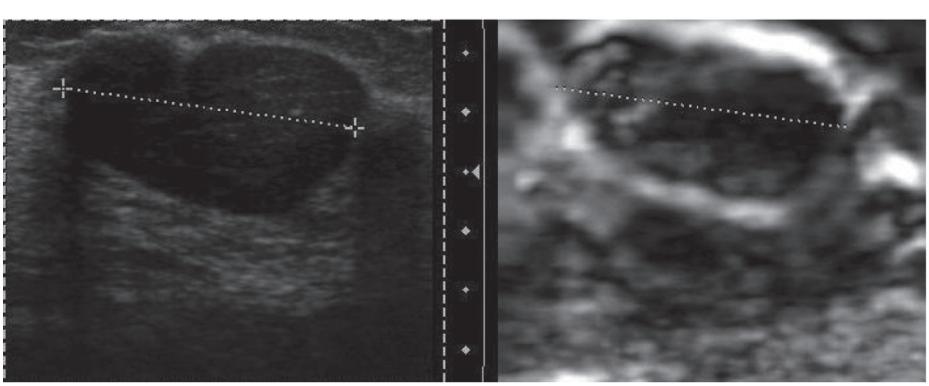
4. RESULTS AND DISCUSSION

In real time clinical diagnosis, elastogram is an ultrasound image which shows relative stiffness of tissues of interest. It is formed by computing the displacement of tissues between post and pre compression images. This real time image contains lot of noises generated by signal processing algorithms which were used to find out the displacement estimates. Since the focus of this paper is on analyzing the mechanical aspects of Ultrasound Elastoraphy, we have chosen ideal strain images which are obtained from simulated phantoms of FEA. Axial strain images obtained in FEA simulations, for 2 mm radius (small size) of inclusion at 40 mm depth is shown in Figure 5 for true modulus contrast variation from -40 dB to 40 dB. From the images, we can notice mechanical shadowing effect around the inclusion. There are two types of shadowing namely stain concentration and strain dilution[14] which are appeared at the proximity of an inclusion. For hard inclusions where the inclusion is harder than background (Figs. 5(a)–(e)), strain concentrations consist of an upright cross, and strain dilutions consist of 45° rotated cross. On the other hand, for soft lesions in which the inclusion is softer than background (Figs. 5(g)–(k)), stain images have 45° rotated cross shaped strain concentrations and upright cross shaped strain dilutions.

Delivered by Publishing Technology to Nanyang Technological University
IP: 202.28.23.227 On: Mon, 30 Nov 2015 20:46:17
Copyright: American Scientific Publishers



(a)



(b)

Fig. 4. Clinical elastogram images for (a) malignant (b) benign cancer respectively. Left side shows ultrasound and right side shows corresponding elastogram.

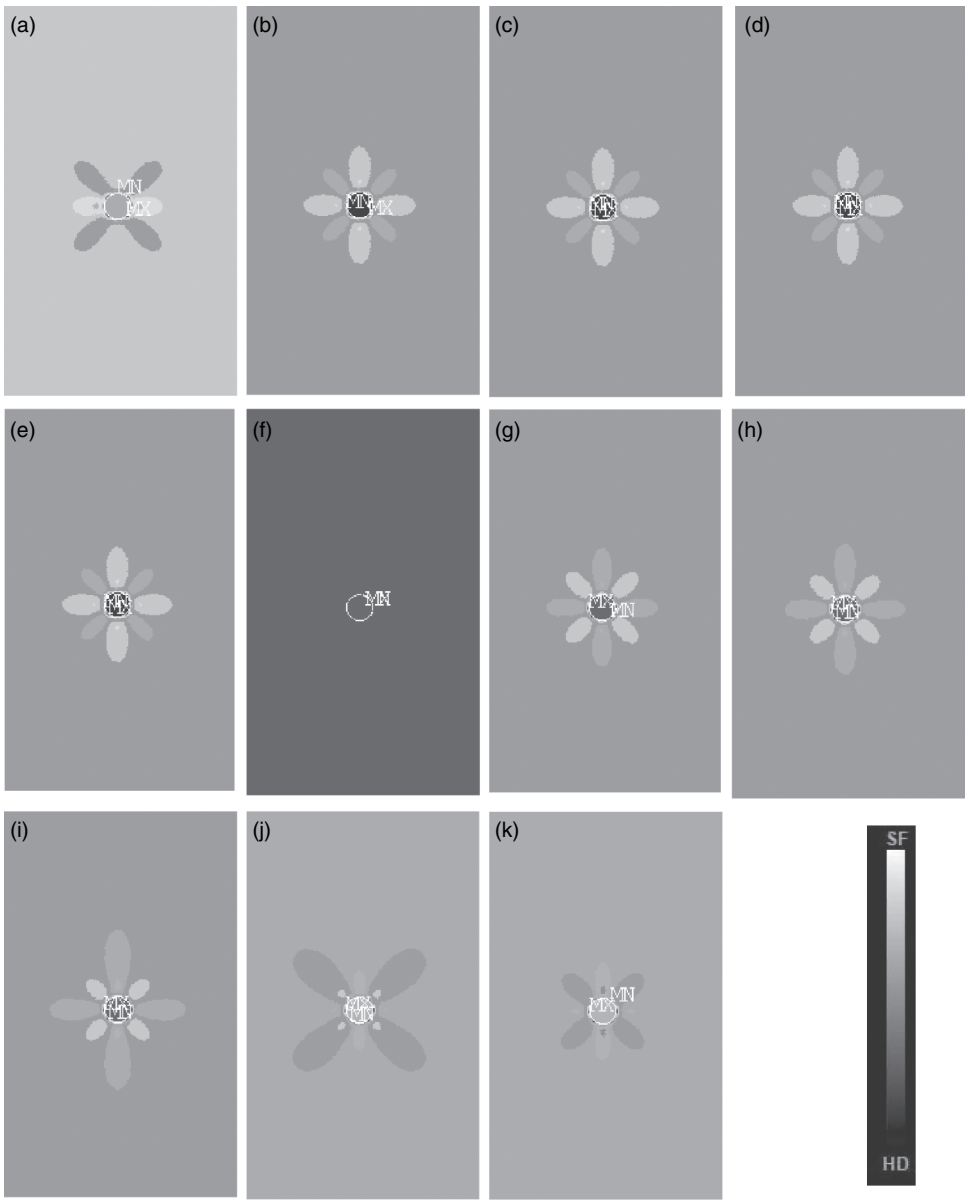


Fig. 5. Strain images for 2 mm radius inclusion with varying true modulus contrast from 40 dB to − 40 dB.

Strain concentrations actually enhance the boundaries of inclusion. For low modulus contrast (less than 6 dB modulus contrast) soft lesion, there is no strain concentration at all. When modulus contrast increases above 6 dB, strain concentrations increases rapidly and reaches a fixed level in high modulus contrast hard inclusion. For small size inclusions, strain concentration could be ignored, while calculating observed contrast. But for large size (8 mm radius) inclusions, strain concentrations occupy most of the background, it was included in calculating background mean strain. For uniformity in ROI selection, for both size inclusions, background ROI was chosen at the same level which covers strain concentration area. Simulation was repeated for inclusions at different depth and strain images were obtained. Since in Ultrasound Elastography, little compression (less than 5%) was applied globally on the top surface of the phantom, they do not show much variation at different depth. Also both displacement and load control produced same set of axial strain images. This might be valid since in the applied compression range (0–5%), the phantom model exhibits pure linear elasticity, the strain contrast depends on only the modulus ratio and do not show any variation with depth and type of load. Moreover, in this linear elasticity range, while calculating CTE, ROIs were chosen at the same spatial location of background and inclusion area in elastogram. The lateral strain profile for small and large size lesion at a fixed modulus contrast and depth are presented in Figure 6. The amplitude of strain concentration remains almost constant for two different size. Due to this, we can notice only a marginal increase in CTE when the diameter of the inclusion was increased from 4 mm to 16 mm. This was expected because the strain in the background settles at almost same level for both inclusions.

Figure 7(a) illustrates the trends of observed contrast with respect to true modulus contrast and (b) demonstrates the variation of CTE for different stiffness inclusions. It is clearly seen

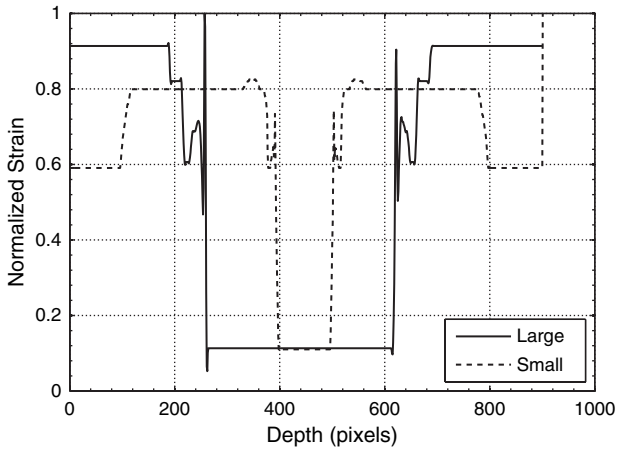


Fig. 6. Lateral strain profile for large and small size inclusions.

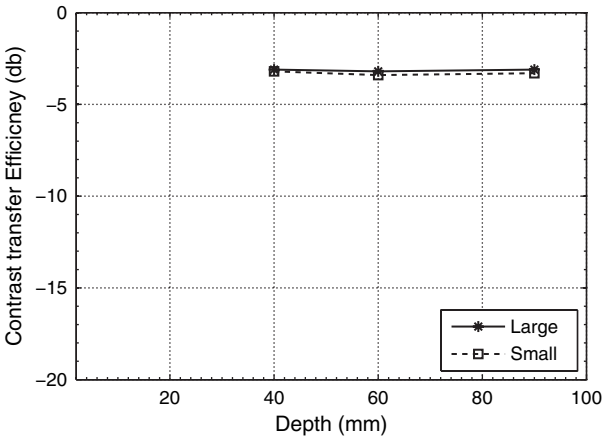


Fig. 8. CTE for large and small lesions at various depth for 20 dB modulus contrast. CTE presents almost constant trend.

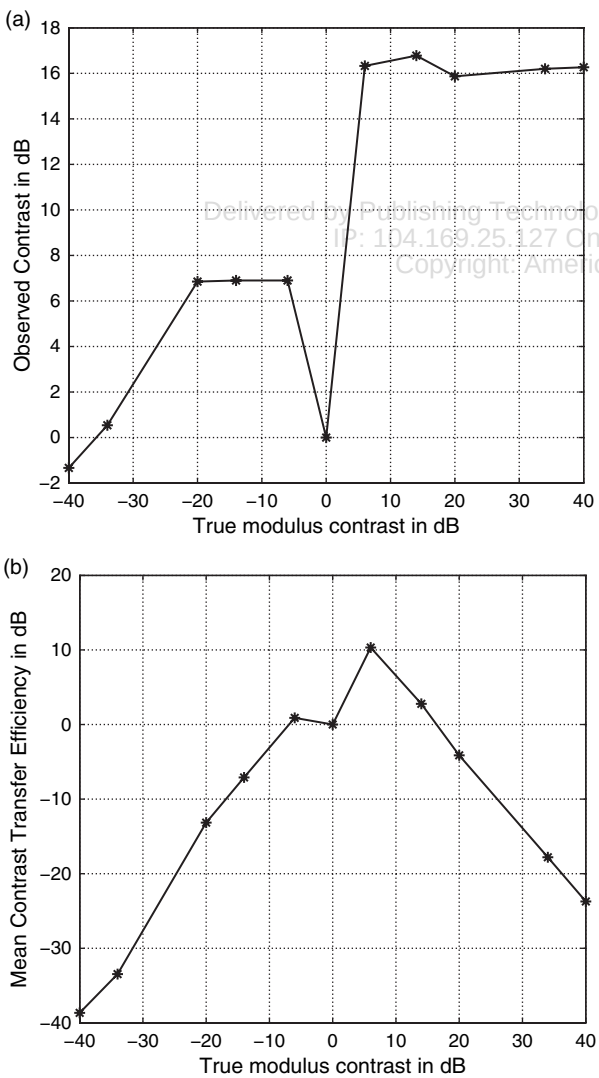


Fig. 7. (a) Observed contrast versus true modulus contrast. (b) CTE versus true modulus contrast.

Delivered by Publishing Technology to: Nanjing Forestry University
IP: 104.169.25.127 On: Mon, 01 Dec 2014
Copyright: American Scientific Publishers

from Figure 7(a) that for both hard and soft lesions of low contrast (less than 6 dB), observed contrast is almost equal to true contrast. However for hard inclusions, when contrast increases, observed contrast reaches a plateau. For soft lesions of high modulus contrast, observed contrast is poor. Same kind of inference could be made in the plot of CTE also. Figure 8 shows the trends of CTE for inclusions at different depth for a modulus contrast of 20 dB. The results are consistent for all the categories of inclusions at different depth and also have good agreement with the results of Ponnekanti et al. 1995.[13]

In this work, all the inclusions are modeled as cylindrical in shape. In reality, the shape of the inclusion might be anything like sphere, rectangle or any irregular shape. However, considering that most of the breast tumors can be approximated to have a cylindrical[2] shape, we did not consider other shapes.

For clinical images, observed strain contrast was calculated by following the procedure used for simulated images. Both benign and malignant class of tumors are considered as hard inclusions in which benign lesions are low modulus contrast lesions and malignant lesions are high modulus contrast inclusions. In clinical elastograhy, there is no possibility of getting true modulus contrast of underlying lesion. However, Kallel et al. 1996[18] derived an analytic expression which relates true modulus contrast (C_m) and observed strain contrast (C_s) which is stated below.

$$\frac{1}{C_s} = \frac{(1-2\nu)}{C_m+(1-2\nu)} + \frac{2}{1+C_m(3-4\nu)} \tag{7}$$

where ν is the Poisson's ratio of both the inclusion and background. For incompressible materials ($\nu = 0.5$), the above equation is reduced to

$$C_s = \frac{1+C_m}{2} \tag{8}$$

The true modulus contrast was calculated for all the 30 cases and CTE is plotted against the calculated true modulus contrast (Fig. 9). As expected, the benign lesions have good CTE than malignant lesions. In the sense, that Ultrasound Elastography should not over exaggerate and in meanwhile it should not under estimate the underlying tissue modulus contrast. Observed contrast should be such that it atleast approximately reaches the true modulus contrast. Otherwise, it will lead to unnecessary confusions. Hence, we can conclude that Ultrasound Elastography is efficient in depicting low contrast lesions than high contrast

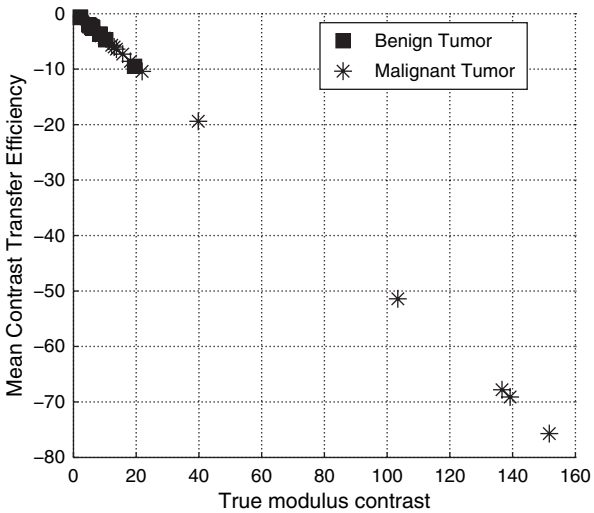


Fig. 9. CTE analysis for clinical elastogram.

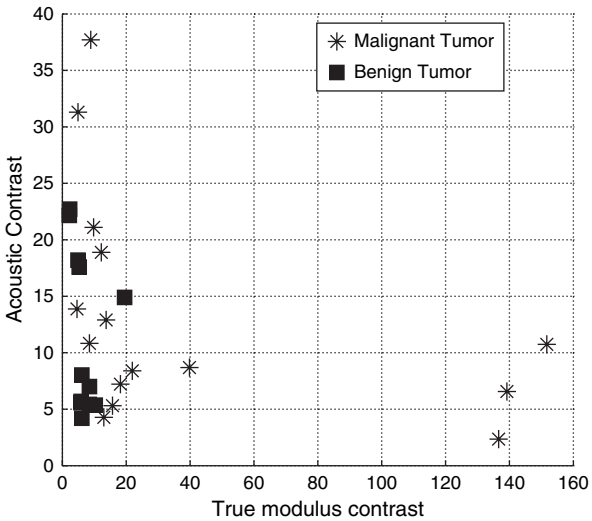


Fig. 11. Acoustic contrast versus true modulus contrast for clinical ultrasound images of malignant and benign tumors.

lesions. More precisely, in hard inclusions for higher modulus ratio, it reaches a limitation in displaying the strain. However, in Ultrasound Elastography more understanding is still required to study the strain concentration and dilution pattern occurring at the interface of the inclusion and background so that the results could be perfectly corroborated with clinical images.

Sample elastogram images of sebaceous cyst and abscess are shown in Figure 10. Understanding the pathological basis for elastographic features of soft lesions is still a challenging task. We attempted to characterize the CTE of elastograms of soft lesions of 10 patients in which the results are conflicting. This might be due to rapid decorrelation of soft inclusion inside stiff matter, they can appear relatively stiff or soft in elastograms, often depending on how much strain applied. From Figure 10 it is evident that soft lesions can have a variety of appearances in elastograms. This is the major disadvantage of linear material model which leads to design a model in which strain contrast is dependent on applied strain.

For completeness, the acoustic contrast for all the ultrasound images of 30 patients are calculated and plotted against the estimated elastic contrast in Figure 11. It shows complete decorrelation between the two properties which states that acoustic contrast is completely independent of stiffness of lesions.

Delivered by Ingenta to: Nanyang Technological University
IP: 155.69.4.4 On: Mon, 14 Jul 2014 08:01:23
Copyright: American Scientific Publishers

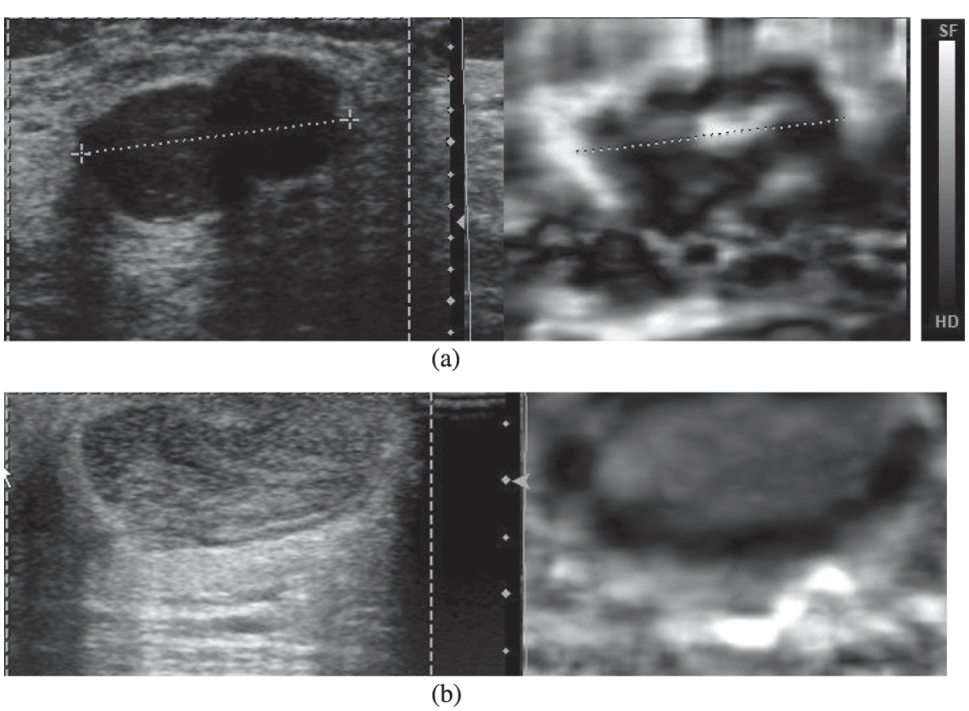


Fig. 10. Clinical elastogram images of soft lesions (a) cyst (b) abscess respectively. Left side shows ultrasound and right side shows corresponding elastogram.

In addition to that, the acoustic contrast features are overlapped among the two categories of lesions which shows the inability of ultrasound *B* mode imaging in differentiation of different types of tumors.

5. CONCLUSION

In this work, tissue mimicking phantoms were simulated using FEA for various modulus contrast inclusions at different depth and of various sizes. Strain images were obtained and contrast of inclusion to the background was calculated. The efficiency of Ultrasound Elasotgrahy in depicting the actual modulus contrast was demonstrated. It is studied that for low modulus contrast lesions, CTE is high and it is getting poor when modulus contrast is increased. The results are also comparable with existing literature and verified with clinical patient images. However, more analysis is required to study the strain concentration at the incision boundary.

Acknowledgment: Two anonymous reviewers are greatly thanked for their very thorough and inspiring review, which substantially improved the manuscript.

References and Notes

1. Y. Zhou, Ultrasound diagnosis of breast cancer. *J. Med. Imaging Health Inf.* 2, 157 **(2013)**.
2. A. T. Stavros, D. Thickman, C. L. Rapp, M. A. Dennis, and S. H. Parker, Solid breast nodules: Use of sonography to distinguish between benign and malignant lesions. *Radiology* 196, 123 **(1995)**.
3. J. Ophir, Elastography: A quantitative method for imaging the elasticity of biological tissues. *Ultrasound Imaging* 13, 111 **(1991)**.
4. M. F. Insana, T. J. Hall, P. Chaturvedi, and C. Kargel, Ultrasonic properties of random media under uniaxial loading. *Journal of Acoustic Society of America* 110, 3243 **(2001)**.
5. L. Wilson and D. Robinson, Ultrasonic measurement of small displacements and deformations of tissue. *Ultrasound Imaging* 4, 71 **(1982)**.
6. R. Dickinson and C. Hill, Measurement of soft tissue motion using correlation between A-scans. *Ultrasound in Medicine and Biology* 8, 263 **(1982)**.
7. R. M. Lerner, K. J. Parker, J. Holen, R. Gramiak, and R. C. Waag, Sono-elasticity: Medical elasticity images derived from ultrasound signals in mechanically vibrated targets. *Acostic Imaging* 16, 317 **(1988)**.
8. T. Sugimoto, S. Ueha, and K. Itoh, Tissue hardness measurement using the radiation force of focused ultrasound. *Proc. Ultrasonics Symposium*, IEEE, Honolulu, HI **(1990)**, Vols. 1377–1380.
9. R. Muthupillai, D. J. Lomas, P. Rossman, J. F. Greenleaf, A. Manduca, and R. L. Ehman, Magnetic resonance elastography by direct visualization of propagating acoustic strain waves. *Science* 269, 1854 **(1995)**.
10. W. Gervals, N. Engene, and C. BkZhou, Breast elastographhy: A perspective Review. *J. Med. Imaging Health Inf.* 1, 1 **(2013)**.
11. C. Usha Devi, R. M. Vasu, and A. K. Sood, Application of ultrasound-tagged photons for measurement of amplitude of vibration of tissue caused by ultrasound: Theory, simulation, and experiments. *J. Biomedical Optics* 11, 1 **(2006)**.
12. W. A. Berg, C. I. Campassi, and O. B. Lotte, Cystic lesions of the breast: Sonographic—pathologic correlation. *Radiology* 227, 183 **(2003)**.
13. H. Ponnekanti, J. Ophir, Y. Huang, and I. Cespedes, Fundamental mechanical limitations on the visualization of elasticity contrast in elastography. *Ultrasound in Medicine and Biology* 21, 533 **(1995)**.
14. F. Kallel and J. Ophir, Limits on the contrast of stress-concentrations in elastography. *Ultrasound in Medicine and Biology* 24, 1215 **(1998)**.
15. M. Bilgen and M. F. Insana, Elastostatics of a spherical inclusion in homogenous biological media. *Physics in Medicine and Biology* 43, 1 **(1998)**.
16. Shyam Bharath and T. Varghese, Contrast-transfer improvement for electrode displacement elastogrpahy. *Physics in Medicine and Biology* 51, 6403 **(2006)**.
17. Y. C. Fung, Biomechanics: Mechanical Properties of Living Tissues, Springer Verlog, New York, USA **(1993)**, Chap. 7.
18. F. Kallel, M. Bertrand, and J. Ophir, Fundamental limitations on the contrast-transfer efficiency in elastography: An analytic study. *Ultrasound in Medicine and Biology* 22, 463 **(1996)**.

Delivered by Ingenta to: National Taiwan University
IP: 203.72.169.25.127 On: Mon, 09 Mar 2015 02:21:17
Copyright: American Scientific Publishers

Received: 28 May 2013. Accepted: 20 September 2013.